The EMBO Journal vol.15 no.24 pp.6798–6809, 1996

Crystal structure of the protein serine/threonine phosphatase 2C at 2.0 Å resolution

Amit K.Das, Nicholas R.Helps[1], Patricia T.W.Cohen[1] and David Barford[2]

Laboratory of Molecular Biophysics, University of Oxford, Rex Richards Building, South Parks Road, Oxford OX1 3QU, UK and [1]MRC Protein Phosphorylation Unit, Department of Biochemistry, University of Dundee, Dundee DD1 4HN, UK

[2]Corresponding author

Protein phosphatase 2C (PP2C) is a Mn^{2+}- or Mg^{2+}-dependent protein Ser/Thr phosphatase that is essential for regulating cellular stress responses in eukaryotes. The crystal structure of human PP2C reveals a novel protein fold with a catalytic domain composed of a central β-sandwich that binds two manganese ions, which is surrounded by α-helices. Mn^{2+}-bound water molecules at the binuclear metal centre coordinate the phosphate group of the substrate and provide a nucleophile and general acid in the dephosphorylation reaction. Our model presents a framework for understanding not only the classical Mn^{2+}/Mg^{2+}-dependent protein phosphatases but also the sequence-related domains of mitochondrial pyruvate dehydrogenase phosphatase, the *Bacillus subtilus* phosphatase SpoIIE and a 300-residue domain within yeast adenyl cyclase. The protein architecture and deduced catalytic mechanism are strikingly similar to the PP1, PP2A, PP2B family of protein Ser/Thr phosphatases, with which PP2C shares no sequence similarity, suggestive of convergent evolution of protein Ser/Thr phosphatases.

Keywords: catalytic mechanism/metalloenzyme/ protein phosphatase 2C/signal transduction/ X-ray crystallography

Introduction

Reversible protein phosphorylation is a widespread and diverse means of regulating cellular functions and in particular intracellular signalling pathways triggered by extracellular stimuli that affect cell growth and homeostasis. Within eukaryotic cells, the opposing activities of protein kinases and phosphatases control the level of protein phosphorylation predominantly on serine, threonine and tyrosine residues. Protein phosphatases are composed of four structurally distinct families (Cohen, 1989; Shenolikar, 1994; Barford *et al.*, 1995; Wera and Hemmings, 1995). Two of these catalyse the dephosphorylation of phosphoserine- and phosphothreonine-containing proteins: (i) the PPP family which includes PP1, PP2A and PP2B (also termed calcineurin); and (ii) the PPM family of Mg^{2+}- or Mn^{2+}-dependent PP2C-like enzymes (PP2C is also designated PPM1A to conform with the nomenclature for human Mg^{2+}-dependent protein serine/threonine phosphatase isoforms; Cohen, 1994).

Mammalian PP2C is representative of a large and varied family of protein phosphatases (Figure 1). The occurrence of sequences related to PP2C within proteins of diverse functions and origins suggests that the PP2C protein fold emerged early in evolution. The two isoforms (α and β) of mammalian PP2C (Tamura *et al.*, 1989; Mann *et al.*, 1992; Wenk *et al.*, 1992) exist as monomers of ~43 kDa, whereas yeast (Maeda *et al.*, 1994; Shiozaki *et al.*, 1994) and *Paramecium* PP2C (Klumpp *et al.*, 1994) lack the C-terminal 100 residues characteristic of mammalian PP2C.

In eukaryotes, PP2C has been implicated in a number of cellular processes including reversal of protein kinase cascades that become activated as a result of stress. In mammalian hepatocytes, inhibition of cholesterol and fatty acid biosynthesis mediated by activation of the AMP-activated protein kinase (AMPK), through elevated AMP/ATP ratios and phosphorylation, is reversed by PP2C-catalysed dephosphorylation of AMPK (Moore *et al.*, 1991). In both fission and budding yeast, genetic analyses have implicated PP2C-like protein phosphatases in negatively regulating the PBS2/HOG1-MAP kinase pathway that is activated in response to osmotic and heat shock (Maeda *et al.*, 1994; Shiozaki *et al.*, 1994; Shiozaki and Russell, 1995). Moreover, roles for PP2C in response to stress were identified in *Arabidopsis* where a mutation within the PP2C catalytic domain sequence of the ABI1 gene blocks signal transduction by the plant hormone abscisic acid, which in wild-type plants leads to maintenance of seed dormancy, stomatal closure and growth inhibition (Leung *et al.*, 1994; Meyer *et al.*, 1994). The role of PP2C-like protein phosphatases in regulating stress response pathways is also conserved in prokaryotes. The protein phosphatase SpoIIE controls the sporulation of *Bacillus subtilus* by dephosphorylating an anti-transcription factor SpoIIAA, reversing the actions of the SpoIIAB protein kinase in a process that is governed by the ADP/ATP ratio (Duncan *et al.*, 1995; Bork *et al.*, 1996). Interestingly, the phosphatase domain of SpoIIE is similar to a domain within the RsbU gene product that controls activation of a stress response transcription factor in *B.subtilus* (Wise and Price, 1995).

Within the PPM family, the PP2C domain occurs in numerous structural contexts (Figure 1). For instance in *Arabidopsis*, PP2C encoded by the ABI1 gene contains a putative Ca^{2+}-binding EF hand motif N-terminal to the catalytic domain (Leung *et al.*, 1994; Meyer *et al.*, 1994) whereas another PP2C homologue, KAPP, associates with the receptor protein Ser/Thr kinase, RLK5, and consists of three regions: an N-terminal membrane localization signal, a kinase interaction domain that associates with the phosphorylated receptor, and a C-terminal catalytic domain (Stone *et al.*, 1994). Mammalian mitochondrial pyruvate deydrogenase phosphatase, a Ca^{2+}-stimulated,

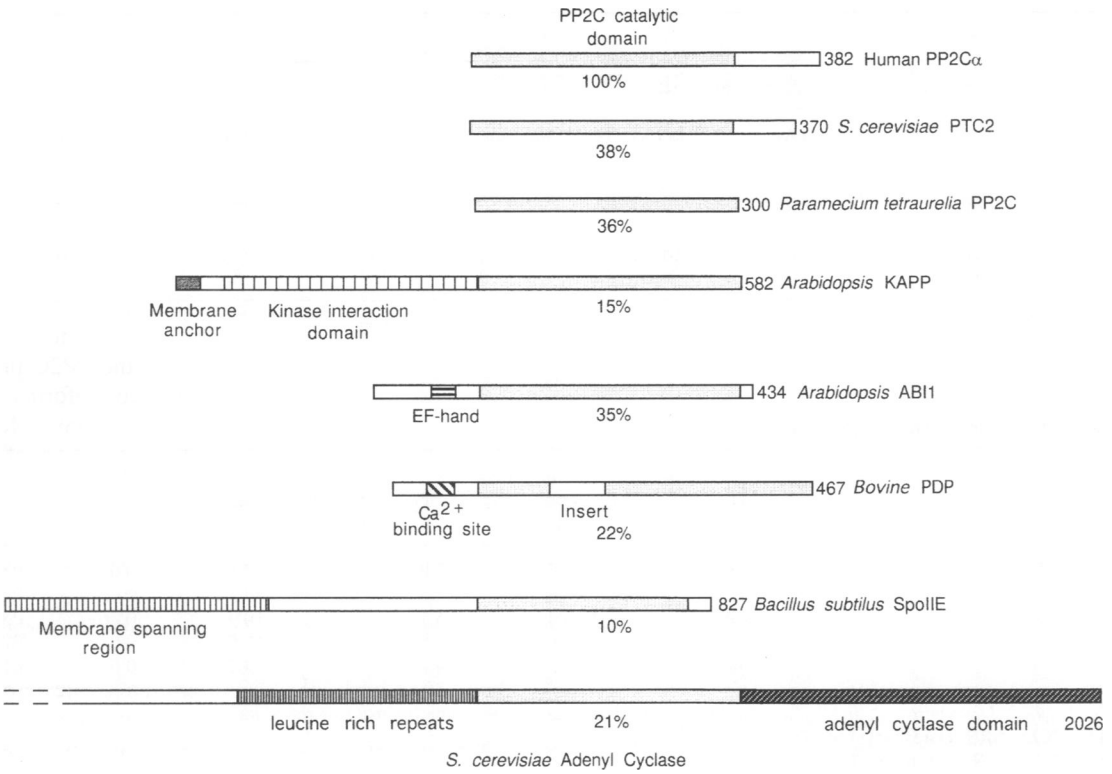

Fig. 1. Structural contexts of the PP2C-like domain. Schematic primary structure of PP2C-like protein phosphatases and the position of the PP2C-like domain within yeast adenyl cyclase. The PP2C domain is shaded light-grey; percentages below indicate sequence identity with human PP2Cα. KAPP: kinase-associated protein phosphatase; PDP: mitochondrial pyruvate dehydrogenase phosphatase. The N-terminal region of *S.cerevisiae* adenyl cyclase is truncated.

Mg^{2+}-dependent protein serine phosphatase that dephosphorylates, thereby activating the pyruvate dehydrogenase multi-enzyme complex, contains a catalytic subunit sharing 22% sequence identity with mammalian PP2C (Lawson *et al.*, 1993). The SpoIIE phosphatase of *B.subtilus* has 10 membrane-spanning regions preceding the catalytic domain (Duncan *et al.*, 1995; Bork *et al.*, 1996). Finally, a 300-residue region of yeast adenyl cyclase, present immediately N-terminal to the cyclase catalytic domain (Kataoka *et al.*, 1985), shares sequence similarity with PP2C (Tamura *et al.*, 1989). This domain may function to mediate ras-GTP activation of adenyl cyclase activity (Coliccelli *et al.*, 1990; Ferger *et al.*, 1991; Minato *et al.*, 1994) and is not known to possess protein phosphatase activity.

The functions of PP2C are likely to encompass processes other than cellular stress responses. For instance, in mammals, five alternatively spliced isoforms of PP2Cβ have been identified that are differentially expressed in different tissues, whereas in budding yeast the PP2C homologue PTC1 is required for correct splicing of tRNAs and cell separation during mitotic growth (Robinson *et al.*, 1994). Determination of the *in vivo* substrates of PP2C has been hampered by the lack of specific PP2C inhibitors. PP2C is unaffected by the naturally occurring inhibitors and toxins that potently inhibit PP1, PP2A and PP2B (Cohen, 1989).

Studies of the crystal structures of protein tyrosine phosphatases (Barford *et al.*, 1994; Stuckey *et al.*, 1994; Su *et al.*, 1994; Zhang *et al.*, 1994) and the PPP family of protein Ser/Thr phosphatases (Egloff *et al.*, 1995; Goldberg *et al.*, 1995; Griffith *et al.*, 1995; Kissinger *et al.*, 1995) coupled with kinetic investigations of these enzymes (Martin and Graves, 1994; Zhang and Dixon, 1994; Zhou *et al.*, 1994) have provided insights into the mechanisms of substrate specificity, catalysis and regulation. In contrast, little is known regarding the structure and catalytic mechanism of PP2C. Here, we describe the crystal structure of human PP2C, which reveals a novel architecture with a catalytic site containing a binuclear ion centre. The catalytic mechanism and protein fold are more similar to those of the PPP family of protein Ser/Thr phosphatases, being quite different from those of the protein tyrosine phosphatases. Knowledge of the structure of PP2C should help in the design of specific inhibitors of this enzyme and the generation of inactivating mutants that will assist in delineating the enzyme's *in vivo* substrates. We also provide immunohistochemical evidence that PP2C is located in both the cytoplasm and nucleus of mammalian cells.

Results and discussion

Structure determination

Parameters for human PP2Cα (382-residue) crystals obtained in the presence of phosphate and manganese ions are given in Tables I–IV. Crystallographic phases were determined from the isomorphous differences and anomalous scattering of mercury and selenomethionine derivatives to 2.6 Å resolution (Table II). Interpretation of the electron density map was straightforward and the resultant atomic model was refined to a resolution of

Table I. Crystal parameters

Crystal	Space group	Unit cell parameters						
		a (Å)	*b* (Å)	*c* (Å)	α (°)	β (°)	γ (°)	Z
Native1	$P3_121$	91.02	91.02	105.69	90.0	90.0	120.0	6
EMTS[a]	$P3_121$	91.05	91.05	105.62	90.0	90.0	120.0	6
SeMet[b]	$P3_121$	91.48	91.48	106.28	90.0	90.0	120.0	6
Native2	$P3_121$	91.02	91.02	105.61	90.0	90.0	120.0	6
EDTA	$P3_121$	91.01	91.01	106.02	90.0	90.0	120.0	6

[a]EMTS, ethyl mercurithiosalicylate.
[b]SeMet, selenomethionine.

Table II. Data collection and processing statistics

Data set	Resolution (Å)	Crystals (*N*)	Measurements (*N*)	Unique reflections		Mean *I*/sig*I*	R_{sym}[a]	X-ray source
				Total (*N*)	Complete (%)			
Native1	25–2.6	1	116163	15953	97.8	17.5	0.051	PX95[b]
EMTS	25–2.4	1	141341	19296	93.2	14.5	0.061	PX95
SeMet	12–2.5	1	119834	17104	95.1	10.9	0.067	PX96
Native2	15–2.0	1	215022	33176	95.5	12.6	0.089	BL19[c]
EDTA	20–2.4	1	94233	17112	84.2	14.2	0.063	BL19

[a]R_{sym} $\Sigma_h\Sigma_i|I_{(h)}-I_{i(h)}|/\Sigma_h\Sigma_i I_{i(h)}$ where $I_{i(h)}$ and $I_{(h)}$ are the *i*th and mean measurements of the intensity of reflection *h*.
[b]PX95: Station PX9.5, SRS, Daresbury, UK.
[c]BL19: Station BL19, ESRF, Grenoble, France.

Table III. Phasing statistics

Data set	Heavy atom sites (*N*)	Isomorphous difference		R_{Cullis}[b]	Anomalous difference	
		Phased reflections (*N*)	Phasing power[a]		Phased reflections (*N*)	Phasing power
EMTS	3	15101	2.13	0.511	13227	1.77
SeMet	9	14172	1.73	0.575	11795	2.07

Combined overall mean figure of merit = 0.690 for 15288 phased reflections.
[a]Root mean square ($<F_H>/E$) where F_H is the heavy atom structure factor amplitude and *E* is the residual lack of closure error.
[b]R_{Cullis} $\Sigma_h||F_{PH}-F_P|-F_H|/\Sigma_h|F_{PH}-F_P|$ for centric data where F_{PH} and F_P are the observed structure factor amplitudes for the derivative and native data sets for reflection *h*, respectively. F_H is the calculated heavy atom structure factor amplitude of reflection *h*.

2.0 Å with an R-factor of 0.21 (Figure 2; Table IV). Additionally, data to 2.4 Å resolution were collected from a PP2C crystal where the metal ions had been previously removed by soaking with 2 mM EDTA (Table IV).

PP2C architecture

Mammalian PP2C, with overall dimensions 35×50×55 Å consists of two domains: an N-terminal catalytic domain (residues 1–290) with six α-helices and 11 β-strands, common to all members of the PP2C family, and a 90-residue C-terminal domain of three α-helices, characteristic of mammalian PP2Cs (Figure 3). The architecture of the catalytic domain is dominated by a central buried β-sandwich formed by the association of two anti-parallel β-sheets with strand order 1, 2, 11, 10, 7, 8 and 3, 4, 5, 6, 9 in sheets 1 and 2, respectively. Both β-sheets of the β-sandwich are flanked by a pair of anti-parallel α-helices, which are inserted between the two central β-strands. The polypeptide chain forms four connections between the two β-sheets. Three occur on the top, representing the catalytic side of the β-sandwich, with the result that a prominent 10 Å wide channel is created with β-strands 1, 2, 3, 11 and 10 on one side and β-strands 4–9 on the other side. One side of the channel is dominated by a 60-residue segment that connects strands β8 and β9 and folds into α3 and an extensive loop region possessing no secondary structure. The C-terminus of β11 connects the catalytic domain with α7 of the C-terminal domain, on

Table IV. Refinement statistics

	Crystal structure	
	Native	EDTA-soaked
Resolution range (Å)	6–2.0	8–2.4
R factor[a]	0.214	0.203
No. of reflections	21806	12147
No. of protein atoms	2823	2816
No. of water molecules	203	197
Deviation from ideality (r.m.s.)[b]		
Bond lengths (Å)	0.011	0.009
Bond angles (°)	1.643	1.512
Dihedrals (°)	0.984	0.911
Torsion (°)	24.37	26.27

[a]*R* factor: $\Sigma_h|F_o-F_c|/\Sigma_h F_o$ where F_o and F_c are the observed and calculated structure factor amplitudes of reflection *h*.
[b] r.m.s., root mean square.

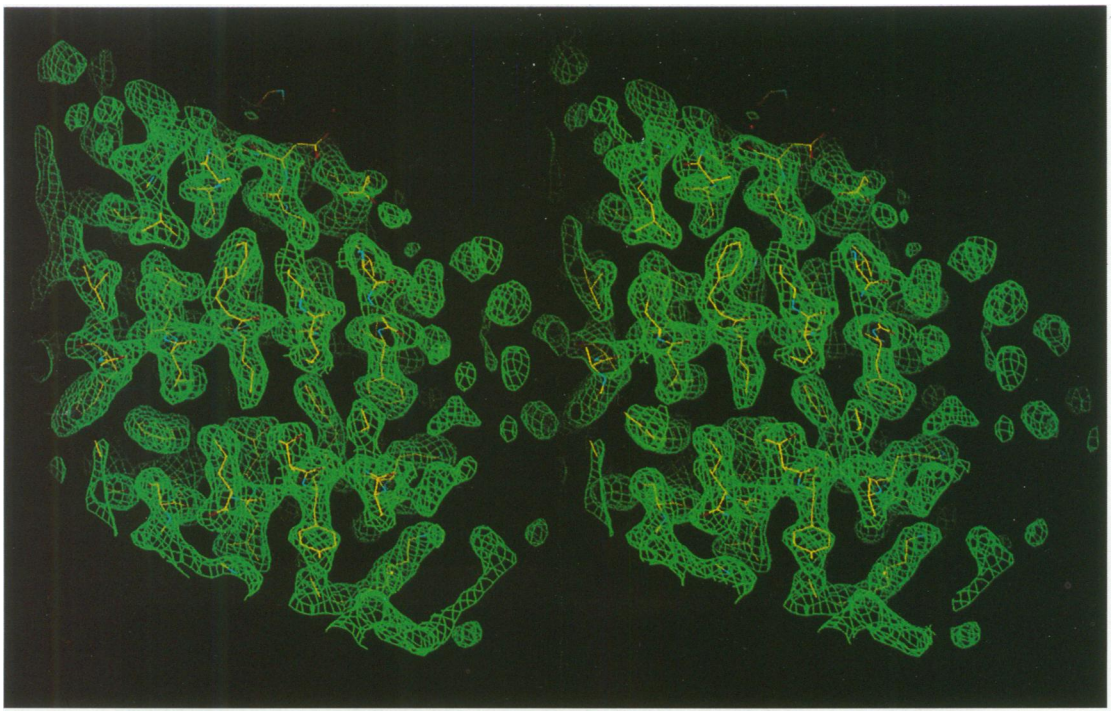

Fig. 2. Stereo view of a portion of the electron density map calculated using ($2F_o$–F_c) coefficients and calculated phases superimposed onto the refined atomic coordinates.

the opposite side of the β-sandwich to the catalytic site. The C-terminal domain is formed from anti-parallel α-helices α7, α8 and α9, with α9 packing against α5 and α6 of the catalytic domain. This domain is remote from the catalytic site and does not appear to play a role in enzyme catalysis, although it may provide protein substrate specificity resulting from the cleft that is created between it and the catalytic domain. Two regions of polypeptide that are not visible in the electron density map are assumed to be disordered. These are residues 322–325, which connect the α-helices α7 and α8, and the C-terminal 18 residues.

To our knowledge, the structure of PP2C is novel. Only the hydrolytic enzymes DNase I (Suck *et al.*, 1984) and exonuclease III (Moi *et al.*, 1996) and the protein Ser/Thr phosphatases PP1 (Egloff *et al.*, 1995; Goldberg *et al.*, 1995) and PP2B (Griffith *et al.*, 1995; Kissinger *et al.*, 1995) have, like PP2C, an architecture organized about a β-sandwich flanked by α-helices with metal ion and substrate-binding sites located at the top of the β-sandwich. However, these proteins differ in their secondary structure topology, indicating different evolutionary origins.

A structure-based multiple sequence alignment of PP2C with the catalytic domains of pyruvate dehydrogenase phosphatase and *B.subtilus* SpoIIE and the PP2C-like domain of yeast adenyl cyclase is shown in Figure 4. Pyruvate dehydrogenase phosphatase and yeast adenyl cyclase share the same secondary structural elements as the PP2C catalytic domain. A 51-residue insert within the pyruvate dehydrogenase phosphatase sequence is accommodated between α1 and α2. Many of the structural features of PP2C are also shared with the *B.subtilus* SpoIIE protein phosphatase; however, in this protein β8 (an edge β-strand of sheet 1) and α3 are deleted. The multiple sequence alignment reveals 10 invariant residues present within eukaryotic PP2Cs, pyruvate dehydrogenase phosphatase and *B.subtilus* SpoIIE phosphatase.

A binuclear metal centre at the catalytic site

A binuclear Mn^{2+} ion site that indirectly coordinates a phosphate ion forms the catalytic site of PP2C located within the channel of the β-sandwich (Figure 3). Many of the invariant residues within the eukaryotic PP2C family and all 10 invariant residues that PP2C shares with pyruvate dehydrogenase phosphatase and *B.subtilus* SpoIIE phosphatase are situated at, or close to, the metal-binding sites (Figure 4). The Mn^{2+} ions were identified both from the electron density values; 12 σ and 9 σ in a $2F_o$–F_c electron density map, for sites 1 and 2, respectively, and the short bond distances (~2.0 Å) to coordinating ligands. The lower electron density corresponding to a metal at site 2 indicates a lower occupancy at this site. Several observations confirm that manganese is bound to the catalytic site in the crystal. First, both sites were modelled reliably as Mn^{2+} during crystallographic refinement. Secondly, proton-induced X-ray emission analysis of PP2C crystals indicated the presence of manganese and the absence of magnesium bound to the protein. The electron density maps calculated using data collected from PP2C crystals incubated for 12 h with 2 mM EDTA indicated dissociation of the metal ions and accompanying water molecules and phosphate ion from the catalytic site. Refinement of the metal-free PP2C structure revealed that it was virtually identical to the holoenzyme form with a root mean square deviation of 0.4 Å between all atoms, indicating that metal ions are not essential for stabilizing the protein fold. Small conformational changes of ~0.5 Å of the carboxylate side chains of Asp60, Asp239 and Asp282 result from loss of metal ions and the

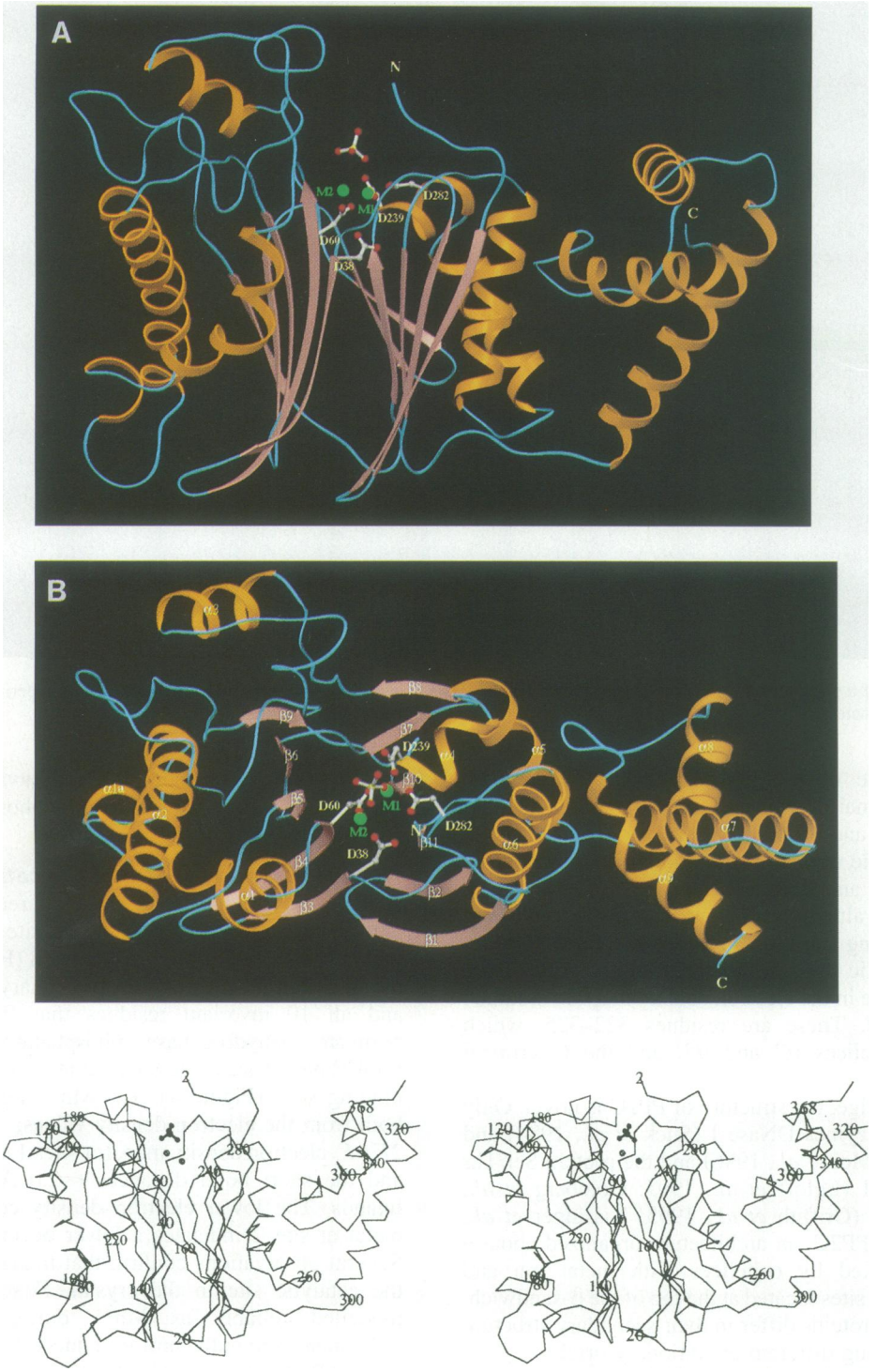

Fig. 3. Two orthogonal views of a ribbon representation indicating the secondary structural elements of PP2C. Invariant metal-coordinating residues Asp38, Asp60, Asp239 and Asp282, the two manganese ions (as green spheres) and the phosphate ion are shown. (**A**) Viewed onto the edge of the β-sandwich structure and (**B**) perpendicular to (A) onto the catalytic site at the top of the β-sandwich structure. Figure produced using SETOR (Evans, 1993). (**C**) Stereo view of a Cα trace of PP2C. The Mn^{2+} (as spheres) and phosphate ions are shown. Drawn using MOLSCRIPT (Kraulis, 1991).

guanidinium group of Arg33 shifts by 1 Å in response to phosphate dissociation.

The binuclear metal centre bridges the two β-sheets of the protein with the Mn^{2+} ions coordinated by residues situated within the β-sandwich structure (Figure 3). Invariant Asp and Glu residues create the metal-binding sites by forming direct coordination bonds to the metal ions and by hydrogen bonding to metal-bound water molecules (Figure 5). The manganese ions are separated by 4.0 Å, the close proximity being facilitated by bridging oxygen atoms. Each ion is hexa-coordinated by oxygen atoms from protein residues and water molecules. A total of six

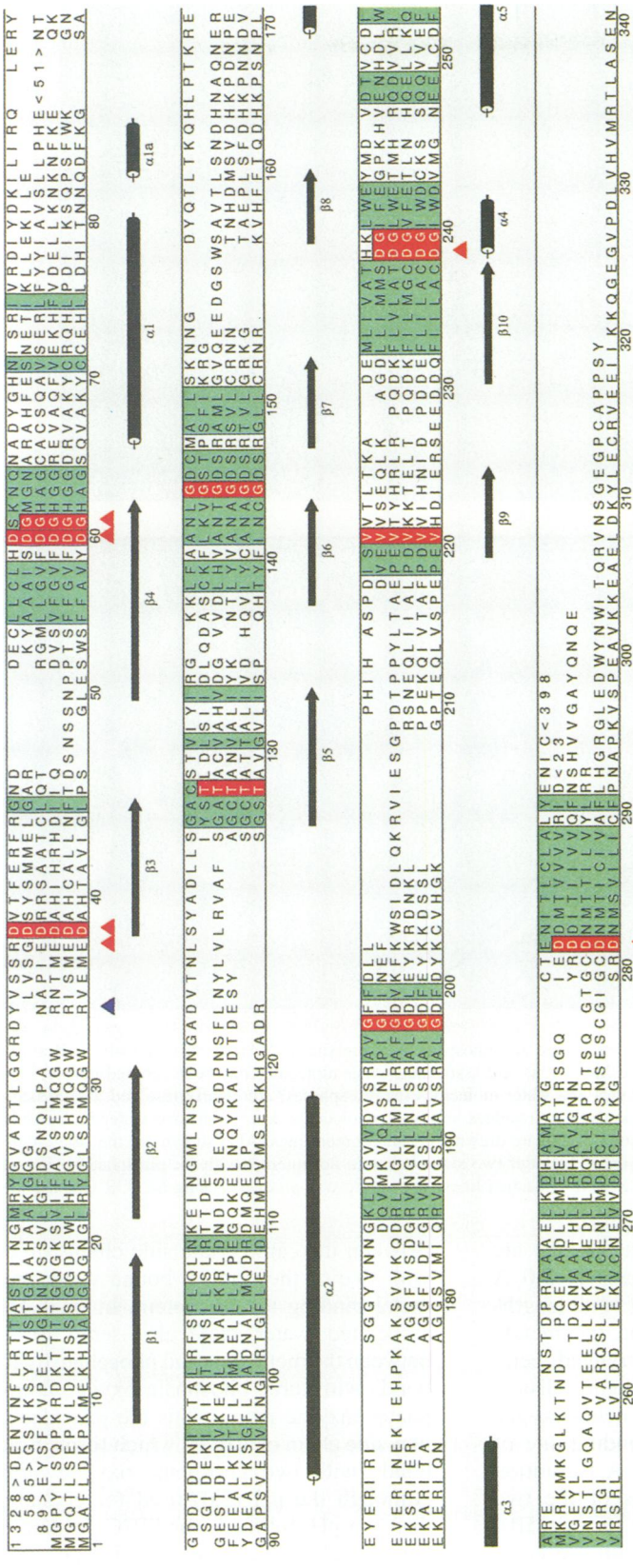

Fig. 4. Multiple sequence alignment of human PP2Cα with the phosphatase catalytic domains of *S.cerevisiae* PTC2, *Paramecium tetraurelia* PP2C, bovine mitochondrial pyruvate dehydrogenase phosphatase, *B.subtilus* SpoIIE gene product and a PP2C-like domain within *S.cerevisiae* adenyl cyclase. Residues that are invariant either in all sequences or within the phosphatase sequences (i.e. not including yeast adenyl cyclase) are coloured red. Conserved residues are shown in green. Residues binding the metal ions and phosphate ions are indicated by red and blue arrows, respectively. The residue numbers correspond to human PP2Cα. The alignment was performed using AMPS (Barton and Sternberg, 1987) and analysed with AMAS (Livingston and Barton, 1993). Alignment of the SpoIIE protein phosphatase sequence is based on Bork *et al.* (1996). The figure was produced using ALSCRIPT (Barton, 1993).

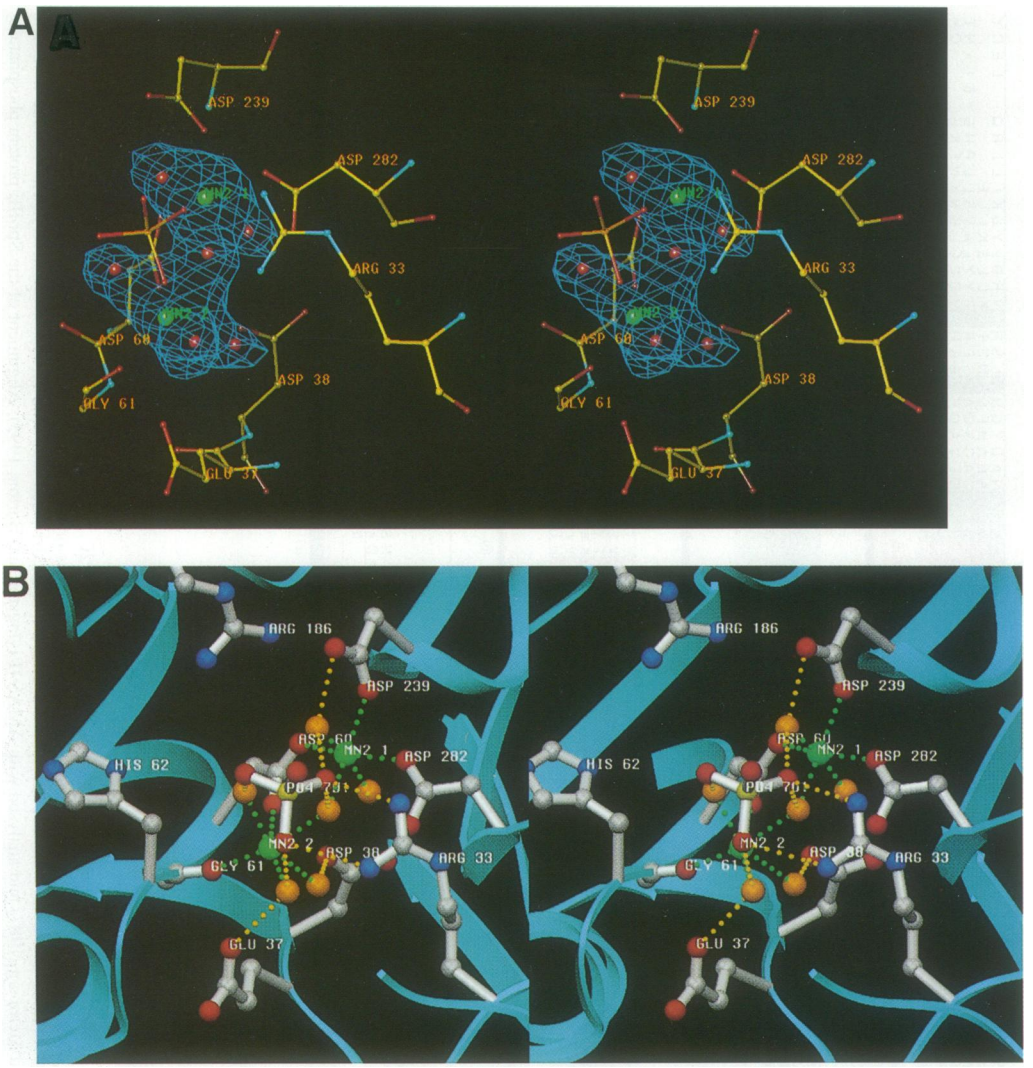

Fig. 5. Stereo views showing details of the binuclear metal centre and phosphate-binding site. (**A**) An electron density omit map using (F_o–F_c) coefficients calculated from a model of PP2C where the Mn^{2+} ions and associated water molecules had been omitted during a simulated annealing refinement (Brunger, 1992). The position of the Mn^{2+} ions and water molecules (as red spheres) are clearly resolved. (**B**) Structure of the phosphate-binding site at the binuclear metal centre with metal-coordinating residues and water molecules. Mn^{2+} ions and water molecules are shown as green and gold spheres, respectively. Metal–oxygen coordination bonds are drawn as dashed green lines. Also shown are the side-chains of Arg33, which forms H-bonds with the phosphate ion, His62 and Arg186. The latter two side chains do not interact with the phosphate, being ~5 Å from the oxygens of the phosphate. Hydrogen bonds are drawn as yellow dashed lines. The figure was produced using SETOR (Evans, 1993).

water molecules that coordinate the two metal ions are clearly resolved in the electron density maps at 2.0 Å resolution (Figure 5A and B). Metal–oxygen bond lengths range from 1.8 Å to 2.3 Å (Figure 6) and the metal–ligand coordination at the two sites is arranged octahedrally, although the geometry at site 2 is slightly distorted. Similar hexa-coordinate geometry and metal–oxygen bond lengths were reported at the Mn^{2+}-binding site of the catalytic site of PP1 determined at 2.1 Å resolution (Goldberg *et al.*, 1995). The environments of the two metal ions at the PP2C catalytic site differ (Figure 5B); Mn^{2+} at site 1 forms direct coordination with the carboxylate groups of three aspartate residues: Asp60, Asp239 and Asp282, while Mn^{2+} at site 2 forms only one direct contact to a carboxylate side chain, that of Asp60. Three water molecules coordinate Mn^{2+} at site 1, one of which is shared with Mn^{2+} at site 2. The four other ligand coordinations to the metal at site 2 are the carbonyl oxygen of Gly61 and three water molecules. Hydrogen bonds between the carboxylate side chains of Glu37 and Asp38 with two of these metal-bound water molecules stabilize metal binding to the protein. In total, four of the metal-associated water molecules serve to mediate contacts between the metal ions and phosphate by forming hydrogen bonds with three phosphate oxygen atoms. Further phosphate–enzyme interactions are provided by the guanidinium side chain of Arg33, which forms bifurcated hydrogen bonds with two phosphate oxygen atoms (Figure 5B). Although the pH (5.0) used for crystal growth is lower than the pH optimum for PP2C, kinetic data suggest that the phosphate site occupied in the crystal represents a physiological substrate-binding site. The enzyme catalyses hydrolysis of *p*-nitrophenol phosphate at pH 5.0, which is competitively inhibited by inorganic phosphate at a rate ~10% of that observed at pH 7.5.

Eukaryotic PP2C, mitochondrial pyruvate dehydrogenase phosphatase and *B.subtilis* SpoIIE phosphatase share every metal-binding residue, except Glu37 (Figure

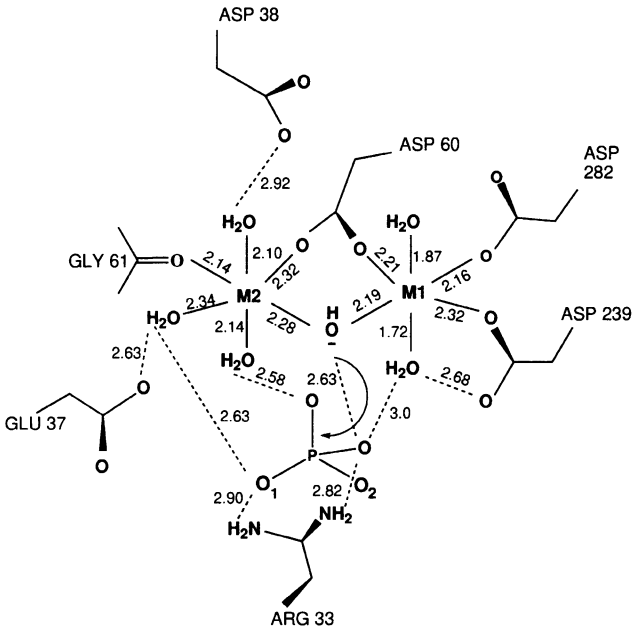

Fig. 6. Schematic of the proposed reaction mechanism catalysed by PP2C. A metal-associated water molecule acts as a nucleophile to attack the phosphorus atom in an S_N2 mechanism while a second water molecule protonates the seryl leaving group oxygen atom. Metal–ligand and H-bond distances are given in Å.

4), suggesting a conserved metal-binding site and a common mechanism of phosphate recognition by the metal ions. Dissociation of metal ions from the catalytic site, using EDTA, inactivates the enzyme and, as revealed from the electron density maps of the PP2C–EDTA crystal structure, abolishes phosphate binding (Table IV). Also striking is the invariance of Thr128 and Gly240, a finding that is explained with our structure since both residues contribute to the structure of the metal-binding sites. The side chain of Thr128 forms a hydrogen bond with the main-chain NH of Asp60, an interaction that presumably stabilizes the coordination of both Mn^{2+} ions by the side chain of Asp60. Gly240 is adjacent to the metal-coordinating residue, Asp239.

Arg33, although invariant within eukaryotic PP2C, is not conserved within the pyruvate dehydrogenase phosphatase and *B.subtilus* SpoIIE sequences, suggesting that in these latter two enzymes either the phosphate–arginine interaction is unnecessary, or that a compensating residue from elsewhere in the structure coordinates the phosphate ion.

Metal ion-catalysed dephosphorylation

PP2C-like protein phosphatases are dependent on either Mg^{2+} or Mn^{2+} for catalytic activity. Mn^{2+} stimulates *B.subtilus* SpoIIE protein phosphatase (Duncan *et al.*, 1995) and is effective at stimulating mammalian PP2C at a concentration 5-fold lower than that of Mg^{2+} (Pato and Kerc, 1991). Other ions such as Ca^{2+}, Zn^{2+} and Ni^{2+} inactivate the enzyme by competitively inhibiting Mn^{2+} or Mg^{2+} binding (Pato and Kerc, 1991). Relatively little is known about the catalytic mechanism of PP2C-like protein phosphatases. The structure of PP2C reported here reveals a dominant role for the binuclear metal centre in substrate recognition and catalysis. The phosphate group of the substrate is coordinated to the enzyme via three phosphate oxygens through hydrogen bonds to metal-bound water molecules. Reduction of the pK_as of water molecules coordinated to Mn^{2+} ions suggests that the metal-bound water molecules at the catalytic site of PP2C could participate in catalysis as nucleophiles and general acids. The structure suggests that a plausible nucleophile is the metal-bridging water molecule, situated 3.7 Å from the substrate phosphorus atom, which could attack the phosphorus atom in an S_N2 mechanism (Figure 6). Coordination to two Mn^{2+} ions may stabilize the more nucleophilic hydroxide ion species. Alternatively, one of the other three metal–phosphate oxygen bridging water molecules, which are within 4.0 Å of the phosphorus atom of the phosphate, may play a role as a nucleophile. Two of the phosphate oxygen atoms appear sufficiently accessible to solvent to be candidate seryl or threonyl side-chain oxygen atoms. One (O2), which lies directly opposite the metal-bridging water molecule, is not coordinated by either protein atoms or water molecules and therefore if this atom corresponded to the leaving group atom, stabilization of the developing negative charge would not occur. The other oxygen atom (O1) forms a hydrogen bond to a metal-bridging water molecule that also hydrogen bonds to the side chain of Glu37. Protein dephosphorylation would be facilitated by protonation of the oxygen atom of the P–O scissile bond. This could be achieved by the metal-bound water molecule that hydrogen bonds to this phosphate oxygen atom. Reduced catalytic activity at pH 5.0 probably results from protonation of a titratable group that acts as a nucleophile. The absence of direct metal–phosphate interactions in PP2C indicates that, in contrast to most other metalloenzymes catalysing phosphorus–oxygen bond cleavage, the metal ions do not polarize the substrate to increase the electrophilic properties of the phosphorus atom or directly stabilize the negative charge on the leaving group oxygen atom.

Our proposal for a catalytic mechanism involving metal-coordinated water molecules accounts for the catalytic site structure where, except for the salt bridge with the side chain of Arg33, no amino acid residues coordinate the phosphate ion either directly or via indirect water-mediated contacts. The mechanism also explains the finding that the only invariant catalytic site residues among PP2C-like protein phosphatases from bacteria to humans participate in metal ion coordination. It is interesting to note that the mutation in the *Arabidopsis* ABI1 gene product (Gly180→Asp) that blocks abscisic acid signalling occurs at a position equivalent to Ala63 of human PP2Cα. Such a substitution might be expected to disrupt the conformation of the metal-coordinating residues Asp60 and Gly61 with concomitant reduction in catalytic activity.

Substrate specificity

In vitro kinetic studies of PP2C using synthetic peptides have revealed that Glu residues immediately flanking the phosphorylated Ser/Thr residue, or proline residues on the C-terminal side, are inhibitory to the dephosphorylation (Donella Deana *et al.*, 1990). Since the catalytic site channel is characterized by a negatively charged electrostatic potential resulting from the preponderance of Asp and Glu residues, many of which are invariant among eukaryotic PP2Cs (Figures 4 and 7), this would disfavour dephosphorylation of peptides containing Asp or Glu. The

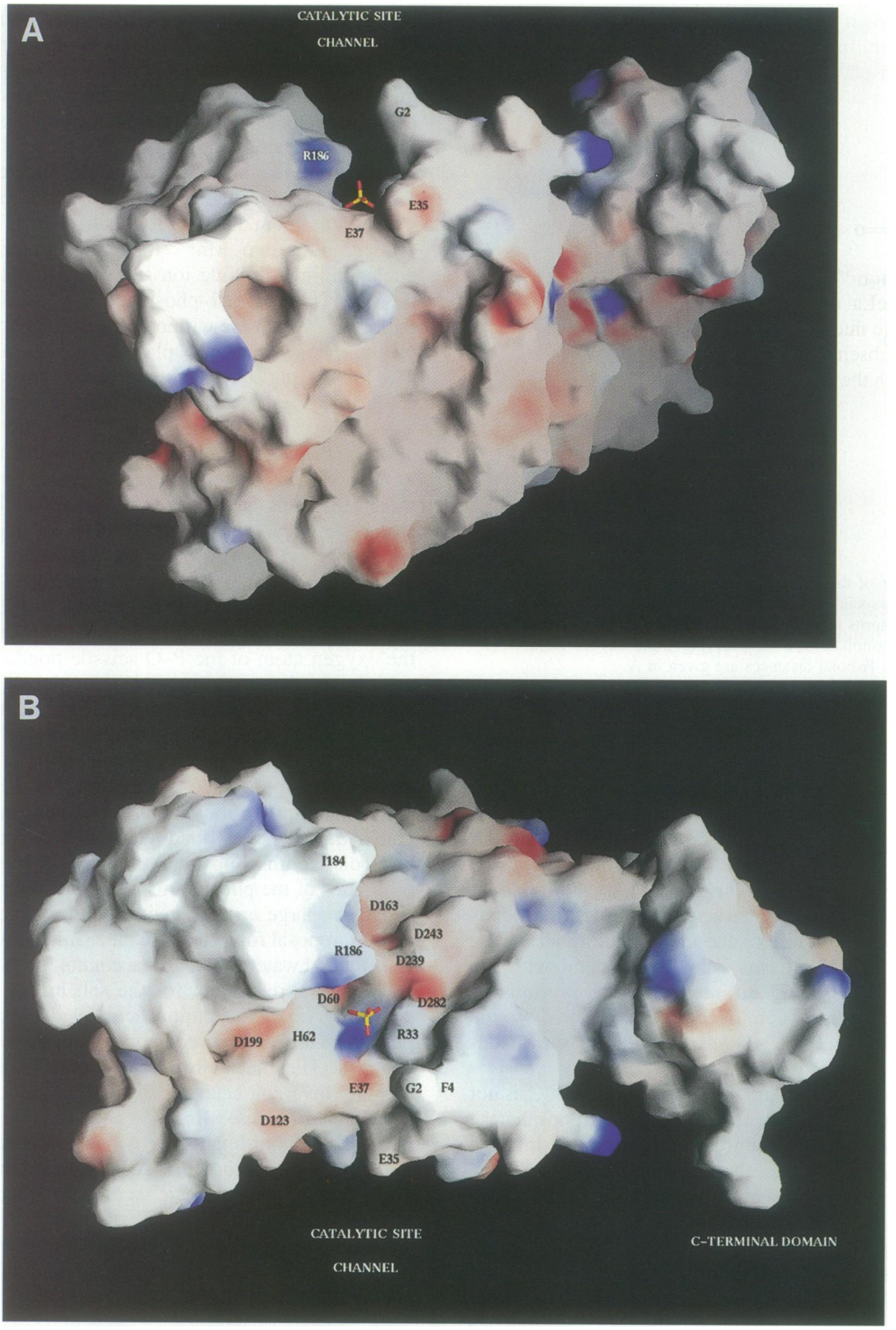

Fig. 7. View of the surface topology of PP2C showing the solvent-accessible surface and surface electrostatic potential. The protein surface is coloured according to the electrostatic potential ranging from blue (most positive) to white (neutral) and red (most negative). The phosphate ion is shown within the catalytic site channel that is surrounded by negative electrostatic potential. Surface residues surrounding the catalytic site are labelled. The protein orientations in (**A**) and (**B**) are similar to those of Figure 3A and B, respectively. The figure was produced using GRASP (Nicholls and Honig, 1991).

presence of the two Mn^{2+} ions and Arg33 creates a local positive electrostatic potential on the protein for recognition of the phosphate group of the substrate. Model-building studies indicate that the position of the phosphate group on the protein surface is consistent with dephosphorylation of residues phosphorylated on Ser, Thr and His residues (Kim *et al.*, 1993). *In vitro*, PP2C displays a 20-fold preference for phosphothreonine-containing substrates compared with equivalent phosphoserine substrates (Donella Deana *et al.*, 1990), which correlates with the

finding that known (Moore *et al.*, 1991) and likely (Maeda *et al.*, 1994; Shiozaki *et al.*, 1994) *in vivo* substrates of PP2C are phosphorylated on phosphothreonine. Understanding the structural basis for this preference and the absence of PP2C activity towards phosphotyrosine proteins requires a crystal structure of a PP2C–peptide complex.

Although PP2C was originally identified in the cytosol of mammalian cells (Cohen, 1989; Shenolika *et al.*, 1994), immunohistochemical analysis shows that it is also present in the nucleus. In MRC5 and GM38 human fibroblasts the nuclear stain was stronger than the cytoplasmic stain, whereas in HeLa cells the cytoplasmic stain was more intense than the nuclear stain (data not shown). In all cells staining was absent from the nucleolus. The occurrence of PP2C in both the cytoplasm and the nucleus is consistent with a role in dephosphorylating components of stress-activated pathways.

Structural relationship to yeast adenyl cyclase

Mutagenesis studies have shown that the PP2C-like domain of *Saccharomyces cerevisiae* adenyl cyclase is essential for ras–GTP stimulation of adenyl cyclase activity (Coliccelli *et al.*, 1990; Ferger *et al.*, 1991; Minato *et al.*, 1994). The dominant interaction with ras–GTP appears to be within the leucine-rich region immediately preceding the PP2C-like domain (Coliccelli *et al.*, 1990; Minato *et al.*, 1994). Whether a metal ion-binding site will be present within the PP2C-like domain of yeast adenyl cyclase is uncertain. The multiple sequence alignment (Figure 4) reveals that only Asp38 and Asp60 of the binuclear metal-binding site are conserved within yeast adenyl cyclase, although interestingly, other metal-coordinating residues of PP2C are conservatively substituted for residues that possess the ability to coordinate Mg^{2+} or Mn^{2+}. For instance, Asp239 and Asp282 at Mn^{2+} site 1 of PP2C are replaced with His and Glu, respectively, in yeast adenyl cyclase. Mutagenesis data indicate that a functional metal ion-binding site may be conserved within the PP2C-like domain of yeast adenyl cyclase. Substitution of Asp1374 of adenyl cyclase with Asn (equivalent to Asp38 of human PP2Cα) causes a 50-fold reduction in the ability of ras–GTP to activate adenyl cyclase activity (Ferger *et al.*, 1991). This could result from a loss of metal binding that affects the ability of adenyl cyclase to recognize ras–GTP or communicate a ras–GTP-mediated conformational change to the adenyl cyclase catalytic domain. It is plausible that the ras–GTP–adenyl cyclase interaction may involve recognition of the solvent-exposed γ-phosphate of GTP bound to ras (Pai *et al.*, 1989) by the metal-binding sites of the PP2C-like domain of adenyl cyclase.

Relationship to other protein phosphatases

The structural description of the PP2C protein fold, catalytic mechanism and substrate binding presented here allows us to compare the properties of this enzyme with those of other protein phosphatases for which structural data have recently been described (Barford *et al.*, 1994; Stuckey *et al.*, 1994; Su *et al.*, 1994; Zhang *et al.*, 1994; Egloff *et al.*, 1995; Goldberg *et al.*, 1995; Griffith *et al.*, 1995; Kissinger *et al.*, 1995). The two families of protein Ser/Thr phosphatases [the PPP family being represented by PP1 (Egloff *et al.*, 1995; Goldberg *et al.*, 1995) and PP2B (Griffith *et al.*, 1995; Kissinger *et al.*, 1995)] share numerous similarities that are distinct from the two protein tyrosine phosphatase (PTP) families (Barford *et al.*, 1994; Stuckey *et al.*, 1994; Su *et al.*, 1994; Zhang *et al.*, 1994). The protein Ser/Thr phosphatases are metalloenzymes that contain within their catalytic sites a binuclear metal-binding site bridging two β-sheets within a β-sandwich architecture that binds the phosphate ion and catalyses dephosphorylation. Whereas Mn^{2+} bound to PP2C indirectly coordinates a phosphate ion through water molecules, the Fe^{2+} and Mn^{2+} bound to PP1 interact directly with the phosphate oxygens of the substrate (Egloff *et al.*, 1995). Our structural data on PP2C and previous data on PP1 (Egloff *et al.*, 1995; Goldberg *et al.*, 1995) and PP2B (Martin and Graves, 1994; Griffith *et al.*, 1995; Kissinger *et al.*, 1995) suggest that in the protein Ser/Thr phosphatases dephosphorylation is catalysed in a single step by a metal-bound water or hydroxide ion. One difference is that in PP2C a metal-bound water protonates the protein leaving group, while in PP1 and PP2B a histidine residue performs this role (Egloff *et al.*, 1995; Griffiths *et al.*, 1995). The low metal affinity of PP2C (Pato and Kerc, 1991) results in its characteristic metal dependence when assayed *in vitro*, a property not observed with PP1. This may be explained by the structure reported here since the metal ion at site 2 forms only two direct and two water-mediated contacts with the enzyme. The PTPs differ from the protein Ser/Thr phosphatases in containing a central β-sheet surrounded by α-helices (Barford *et al.*, 1994; Stuckey *et al.*, 1994; Su *et al.*, 1994; Zhang *et al.*, 1994). In both families of PTPs the phosphate group of the phosphotyrosine residue is recognized by a conserved phosphate-binding motif that contains a nucleophilic Cys residue that forms a thiophosphate intermediate during the dephosphorylation reaction (Zhang and Dixon, 1994).

Despite the distant evolutionary relationships of protein Ser/Thr phosphatases containing PP2C-like catalytic domains, the conservation of essential metal-coordinating residues, as is revealed by our structural data, suggests that these enzymes share the same fundamental aspects of catalysis. Conservation of metal-binding Asp residues between *B.subtilus* SpoIIE and human PP2Cα confirms the presence of PP2C-like protein phosphatases in prokaryotes. The occurrence of a PP2C-like domain within yeast adenyl cyclase suggests additional functions for this domain. The four families of protein phosphatases have unrelated sequences, yet both the Ser/Thr-specific phosphatases and PTPs represent examples of convergent evolution. The two families of protein Ser/Thr phosphatases are metalloenzymes, share marked structural similarities at the tertiary level, and dephosphorylate their substrates using metal-activated water molecules.

Materials and methods

Protein purification and crystallization

cDNA encoding human PP2Cα was expressed in *Escherichia coli* in the presence of 1 mM Mn^{2+} under the control of the pTactac promoter as described previously (Davies *et al.*, 1995). Protein purification to homogeneity was performed using five purification steps: (i) ammonium sulfate precipitation at 50% (w/v) $(NH_4)_2SO_4$; (ii) Q-Sepharose and (iii) Mono Q anion exchange chromatography; (iv) gel filtration on a Pharmacia Superose 200 column; and (v) hydrophobic interaction chromatography. The purified protein was dialysed into 10 mM Tris–

HCl, pH 7.5, 50 mM NaCl, 1 mM Mn^{2+}, 2 mM DTT and concentrated to 15 mg/ml. Crystallizations were performed at 4°C using the vapour diffusion method by mixing equal volumes of the protein and precipitating solution consisting of 50 mM potassium phosphate, pH 5.0, 8–12% (w/v) polyethylene glycol (mol. wt 8000), 15% (v/v) glycerol and 2 mM DTT. Crystals appeared within 7 days and grew to dimensions 0.2×0.2×1.0 mm. All data were collected at 100 K. Crystals were transferred into a cryoprotection buffer consisting of 50 mM sodium phosphate, pH 5.0, 25 mM NaCl, 13% (w/v) polyethylene glycol (mol. wt 8000), 32% (v/v) glycerol, before flash-freezing in a nitrogen gas stream. PP2C with incorporated selenomethionine was obtained by transforming *E.coli* DL46 cells with the PP2C expression vector and growing the cells in a defined medium as described (Hendrickson *et al.*, 1990). The protein was purified and crystallized as for the wild-type protein.

Structure determination

Mercury derivative crystals were obtained by soaking wild-type PP2C crystals in 1.0 mM ethyl mercurithiosalicylate (EMTS) for 3 h and then back-soaking in crystallization buffer. Native and the EMTS-data sets were collected at PX9.5 SRS, Daresbury and the selenomethionine data were collected at PX9.6 SRS, Daresbury to a resolution of 2.6 Å using MAR image plates. Images were integrated and the data scaled and reduced using DENZO and SCALEPACK (Otwinowski, 1993). Multiple isomorphous replacement anomalous scattering phases were calculated using the PHASES package (Furey and Swaminathan, 1990) and improved using solvent flattening (solvent content of 0.60). The electron density map was interpreted and model building performed by means of O (Jones *et al.*, 1991) and the atomic model was refined using X-PLOR (Brunger, 1992). Subsequently, a 2.0 Å resolution native data set was collected at BL19, ESRF using a charged coupled device detector and the model refined using these data. The EDTA–PP2C data set at 2.4 Å resolution was collected at BL19 from a single crystal that had been soaked for 12 h with 2 mM EDTA before freezing.

Proton-induced X-ray emission spectroscopy

A crystal of PP2C was mounted onto a 5 μm thick sheet of Kimfoil and dried for 12 h. The experimental procedure for data collection has been described previously (Grime *et al.*, 1991; Egloff *et al.*, 1995).

Immunofluorescent localization of PP2C

GM38 human skin fibroblasts (Kuehl *et al.*, 1996), MRC5 human embryonic lung fibroblasts and HeLa cells were fixed in 4% *p*-formaldehyde for 20 min as described (Brewis *et al.*, 1993). Antibodies to bacterially expressed PP2C were raised in sheep and affinity-purified against the whole protein (Brewis *et al.*, 1993). The anti-PP2C antibodies were detected with fluorescein-labelled donkey anti-sheep antibodies. Fluorescent micrographs were taken with a Bio-Rad MRC 600 confocal microscope. DNA was detected by staining with 0.5 μg/ml propidium iodide.

Kinetic experiments

PP2C was assayed under the following conditions; at pH 5.0 with 25 mM MES, 50 mM NaCl, 2 mM $MnCl_2$, 0.1 % β-mercaptoethanol, 25 mM *p*-nitrophenol phosphate and at pH 7.5 with 25 mM Tris–HCl instead of 25 mM MES. Formation of *p*-nitrophenol was observed at 410 nm.

Acknowledgements

We wish to thank our colleagues at PX9.5, PX9.6, SRS Daresbury, UK and at BL19 ESRF, Grenoble, France for help with X-ray data collection and Dr M.-P.Egloff for useful discussions. The work was funded by grants from the Medical Research Council, UK and the Wellcome Trust to D.B. and from the Medical Research Council, UK to P.T.W.C.

References

Barford,D., Flint,A.J. and Tonks,N.K. (1994) Crystal structure of human protein tyrosine phosphatase 1B. *Science*, **263**, 1397–1404.

Barford,D., Jia,Z. and Tonks,N.K. (1995) Protein tyrosine phosphatases take off. *Nature Struct. Biol.*, **2**, 1043–1053.

Barton,G.J. (1993) ALSCRIPT: a tool to format multiple sequence alignments. *Protein Engng*, **6**, 37–40.

Barton,G.J. and Sternberg,M.J.E. (1987) A strategy for the rapid multiple alignment of protein sequences. *J. Mol. Biol.*, **198**, 327–337.

Bork,P., Brown,N.P., Hegyi,H. and Shultz,J. (1996) The protein phosphatase 2C (PP2C) superfamily: detection of bacterial homologues. *Protein Sci.*, **5**, 1421–1425.

Brewis,N.D., Street,A.J., Prescott,A.R. and Cohen,P.T.W. (1993) PPX, a novel protein serine/threonine phosphatase localised to centrosomes. *EMBO J.*, **12**, 987–996..

Brunger,A.T. (1992) X-PLOR: version 3.1. Yale University Press, New Haven, CT.

Cohen,P. (1989) The structure and regulation of protein phosphatases. *Annu. Rev. Biochem.*, **58**, 453–508.

Cohen,P.T.W. (1994) Nomenclature and chromosomal localisation of human protein serine/threonine phosphatase gene. *Adv. Protein Phosphat.*, **8**, 371–376.

Colicelli,J., Field,J., Ballester,R., Chester,N., Young,D. and Wigler,M. (1990) Mutational mapping of ras-responsive domains of the *Saccharomyces cerevisiae* adenylyl cyclase. *Mol. Cell. Biol.*, **10**, 2539–2543.

Davies,S.P., Helps,N.R., Cohen,P.T.W. and Hardie,D.G. (1995) 5′-AMP inhibits dephosphorylation, as well as promoting phosphorylation, of the AMP-activated protein kinase. Studies using bacterially expressed human protein phosphatase 2Cα and PP2AC. *FEBS Lett.*, **377**, 421–425.

Donella Deana,A., McGowan,C.H., Cohen,P., Marciori,F., Meyer,H.E. and Pinna,L.A. (1990) An investigation of the substrate specificity to protein phosphatase 2C using synthetic peptide substrates. Comparison with protein phosphatase 2A. *Biochim. Biophys. Acta*, **1051**, 199–202.

Duncan,L., Alper,S., Arigoni,F., Losick,R. and Stragier,P. (1995) Activation of cell-specific transcription by a serine phosphatase at the site of asymmetric division. *Science*, **270**, 641–644.

Egloff,M.-P., Cohen,P.T.W., Reinemer,P. and Barford,D. (1995) Crystal structure of the catalytic subunit of human protein phosphatase 1 and its complex with tungstate. *J. Mol. Biol.*, **254**, 942–959.

Evans,S.V. (1993) SETOR: hardware lighted three dimensional solid model representation of macromolecules. *J. Mol. Graphics*, **11**, 134–138.

Ferger,G., De Vendittis,E., Vitelli,A., Masturzo,P., Zahn,R., Verrotti,A.C., Kavounis,C., Pal,G.P. and Fasano,O. (1991) Identification of regulatory residues of the yeast adenylyl cyclase. *EMBO J.*, **10**, 349–359.

Furey,W. and Swaminathan,S. (1990) PHASES – a program package for the processing and analysis of diffraction data from macromolecules. *Am. Cryst. Assoc. Meeting Summ.*, **18**, 73.

Goldberg,J., Huang,H., Kwon,Y., Greengard,P., Nairn,A.C. and Kuriyan,J. (1995) Three dimensional structure of the catalytic subunit of protein serine/threonine phosphatase-1. *Nature*, **376**, 745–753.

Griffith,J.P. *et al.* (1995) X-ray structure of calcineurin inhibited by the immunophilin-immunosuppressant FKBP12-FK506 complex. *Cell*, **82**, 507–522.

Grime,G.W., Dawson,M., Marsch,M., McArthur,I.C. and Watt,F. (1991) The Oxford submicron nuclear microscope facility. *Nuclear Instruments and Methods in Physics Research*, **B54**, 52–63.

Hendrickson,W.A., Horton,J.R. and LeMaster,D.M. (1990) Selenomethionyl proteins produced for analysis by multiwavelength anomalous diffraction (MAD): a vehicle for direct determination of three-dimensional structure. *EMBO J.*, **9**, 1665–1758.

Jones,T.A., Zou,J.Y., Cowan,S.W. and Kjeldgaard,M. (1991) Improved methods for building protein models in electron density maps and the location of errors in these models. *Acta Crystallogr.*, **A47**, 110–119.

Kataoka,T., Broek,D. and Wigler,M. (1985) DNA sequence and characterization of the *S. cerevisiae* gene encoding adenylate cyclase. *Cell*, **43**, 493–505.

Kim,Y., Huang,J., Cohen,P. and Matthews,H.R. (1993) Protein phosphatase 1, 2A, and 2C are protein histidine phosphatases. *J. Biol. Chem.*, **268**, 18513–18518.

Kissinger,C.R. *et al.* (1995) Crystal structure of human calcineurin and the human FKBP12-FK506-calcineurin complex. *Nature*, **378**, 641–644.

Klumpp,S., Hanke,C., Donella-Deana,A., Beyer,A., Kellner,R., Pinna,L.A. and Schultz,J.E. (1994) A membrane-bound protein phosphatase type 2C from *Paramecium tetraurelia*. *J. Biol. Chem.*, **269**, 32774–32780.

Kraulis,P. (1991) MOLSCRIPT: a program to produce both detailed and schematic plots of protein structures. *J. Appl. Crystallogr.*, **24**, 946–950.

Kuehl,B.L., Brezden,C.B., Traver,R.D., Sigeel,D., Ross,D., Renzing,J. and Rauth,A.M. (1996) Immortalisation of a human diploid fibroblast cell strain provides a DT/diaphorise paradox. *Br. J. Cancer*, **74**, 519–522.

Lawson,J.E., Niu,X.-D., Browning,K.S., Trong,H.L., Yan,J. and Reed,L.J. (1993) Molecular cloning and expression of the catalytic subunit of bovine pyruvate dehydrogenase phosphatase and sequence similarity with protein phosphatase 2C. *Biochemistry*, **32**, 8987–8993.

Leung,J., Bouvier-Durand,M., Morris,P.-C., Guerrier,D., Chefdor,F. and Giraudat,J. (1994) *Arabidopsis* ABA response gene ABI1: features of a calcium-modulated protein phosphatase. *Science*, **264**, 1448–1452.

Livingston,C.D. and Barton,G.J. (1993) Protein sequence alignments: a strategy for hierarchical analysis of residue conservation. *Comput. Applic. Biosci.*, **9**, 745–756.

Maeda,T., Wurgler-Murphy,S.M. and Saito,H. (1994) A two-component system that regulates an osmosensing MAP kinase cascade in yeast. *Nature*, **369**, 242–245.

Mann,D.J., Campbell,D.G., McGowan,C.H. and Cohen,P.T.W.C. (1992) Mammalian protein serine/threonine phosphatase 2C: cDNA cloning and comparative analysis of amino acid sequence. *Biochim. Biophys. Acta*, **1130**, 100–104.

Martin,B.L. and Graves,D.J. (1994) Isotope effects on the mechanism of calcineurin catalysis: kinetic solvent isotope and isotope exchange studies. *Biochim. Biophys. Acta*, **1206**, 136–142.

Meyer,K., Leube,M.P. and Grill,E. (1994) A protein phosphatase 2C involved in ABA signal transduction in *Arabidopsis thaliana*. *Science*, **264**, 1452–1455.

Minato,T., Wang,J., Akasaka,K., Okada,T., Suzuki,N. and Kataoka,T. (1994) Quantitative analysis of mutually competitive binding of human raf-1 and yeast adenylyl cyclase to ras proteins. *J. Biol. Chem.*, **269**, 20845–20851.

Moi,C.D., Kuo,C.-F., Thayer,M.M., Cunnigham,R.P. and Tainer,J.A. (1996) Structure and function of the multi functional DNA-repair enzyme exonuclease III. *Nature*, **374**, 381–386.

Moore,F., Weekes,J. and Hardie,D.G. (1991) Evidence that AMP triggers phosphorylation as well as direct allosteric activation of rat liver AMP-activated protein kinase. *Eur. J. Biochem.*, **199**, 691–697.

Nicholls,A. and Honig,B. (1991) A rapid finite difference algorithm, utilising successive over relaxation to solve the Poisson–Boltzmann equation. *J. Comput. Chem.*, **12**, 435–445.

Otwinowski,Z. (1993) DENZO. In Sawyer,L., Isaacs,N. and Bailey,S. (eds), *Data Collection and Processing*. SERC Daresbury Laboratory, Warrington, UK, p. 56.

Pai,E.F., Kabsch,W., Krengel,U., Holmes,K.C., John,J. and Wittinghofer,A. (1989) Structure of the guanine-nucleotide-binding domain of the Ha-ras oncogene product p21 in the triphosphate conformation. *Nature*, **341**, 209–214.

Pato,M.D. and Kerc,E. (1991) Regulation of smooth muscle phosphatase-II by divalent cations. *Mol. Cell. Biochem.*, **101**, 31–41.

Robinson,M.K., van Zyl,W.H., Phizicky,E.M. and Broach,J.R. (1994) TPD1 of *Saccharomyces cerevisiae* encodes a protein phosphatase 2C-like activity implicated in tRNA splicing and cell separation. *Mol. Cell. Biol.*, **14**, 3634–3645.

Shenolikar,S. (1994) Protein serine/threonine phosphatases – new avenues for cell regulation. *Annu. Rev. Cell. Biol.*, **10**, 56–86.

Shiozaki,K. and Russell,P. (1995) Counteractive roles of protein phosphatase 2C (PP2C) and a MAP kinase kinase homolog in the osmoregulation of fission yeast. *EMBO J.*, **14**, 492–502.

Shiozaki,K., Akhavan-Niaki,H., McGowan,C.H. and Russell,P. (1994) Protein phosphatase 2C, encoded by ptc1+, is important in the heat shock response of *Schizosaccharomyces pombe*. *Mol. Cell. Biol.*, **14**, 3742–3751.

Stone,J.M., Collinge,M.A., Smith,R.D., Horn,M.A. and Walker,J.C. (1994) Interaction of protein phosphatase with an *Arabidopsis* serine-threonine receptor kinase. *Science*, **266**, 793–795.

Stuckey,J.A., Schubert,H.L., Fauman,E.B., Zhang,Z.-Y., Dixon,J.E. and Saper,M.A. (1994) Crystal structure of yersinia protein tyrosine phosphatase at 2.5 Å and the complex with tungstate. *Nature*, **370**, 571–575.

Su,X.-D., Taddei,N., Stefani,M., Ramponi,G. and Nordlund,P. (1994) The crystal structure of a low-molecular-weight phosphotyrosine protein phosphatase. *Nature*, **370**, 575–578.

Suck,D., Oefner,C. and Kabsch,W. (1984) Three dimensional structure of bovine pancreatic DNase I at 2.5 Å resolution. *EMBO J.*, **3**, 2423–2430.

Tamura,S., Lynch,K.R., Larner,J., Fox,J., Yasui,A., Kikuchi,K., Suzuki,Y. and Tsuiki,S. (1989) Molecular cloning of rat type 2C (IA) protein phosphatase mRNA. *Proc. Natl Acad. Sci. USA*, **86**, 1796–1800.

Wenk,J., Trompeter,H.-I., Pettrich,K.-G., Cohen,P.T.W., Campbell,D.G. and Mieskes,G. (1992) Molecular cloning and primary structure of a protein phosphatase 2C isoform. *FEBS Lett.*, **297**, 135–138.

Wera,S. and Hemmings,B.A. (1995) Serine/threonine protein phosphatases. *Biochem. J.*, **311**, 17–29.

Wise,A.A. and Price,C.W. (1995) Four additional genes in the sigB operon of *Bacillus subtilis* that control activity of the general stress factor sB in response to environmental signals. *J. Bacteriol.*, **177**, 123–133.

Zhang,M., Van Etten,R.L. and Stauffacher,C.V. (1994) Crystal structure of bovine heart phosphotyrosyl phosphatase at 2.2 Å resolution. *Biochemistry*, **33**, 11097–11105.

Zhang,Z.Y. and Dixon,J.E. (1994) Protein tyrosine phosphatases: mechanism of catalysis and substrate specificity. *Adv. Enzymol. Relat. Areas Mol. Biol.*, **68**, 1–38.

Zhou,S., Clemens,J.C., Stone,R.L. and Dixon,J.E. (1994) Mutational analysis of a ser/thr phosphatase. *J. Biol. Chem.*, **269**, 26234–26238.

Received on June 19, 1996; revised on August 1, 1996